Chapter 6

Control Technology of Solidification and Cooling in the Process of Continuous Casting of Steel

Qing Liu, Xiaofeng Zhang, Bin Wang and Bao Wang

Additional information is available at the end of the chapter

http://dx.doi.org/10.5772/51457

1. Introduction

Solidification and cooling control, which is a key technology in the continuous casting process, has a quick development in recent years, and meet the modern requirements of the continuous casting process on the whole. However, the control models and cooling technology need constant development and improvement due to the trend toward delicacy and full automation in continuous casting. This chapter discusses the hot ductility, the thermophysical properties, the solidification and cooling control models and nozzles layouts for secondary cooling, besides these, the planning for the process of steelmaking-rolling, which are closely related with solidification and cooling in continuous casting process.

2. Research on the thermal physical parameters of steels

This section summarizes formulae for calculating thermal physical parameters of steel slabs, including the liquidus temperature, solidus temperature, thermal conductivity, and so on. The database of thermal physical parameters including thermoplastic was specially established and embedded in the control model of the solidification and cooling, which is convenient to query data and update operation for technical staffs. Moreover, based on the thermoplastic parameter database, the target surface control temperature of slab is determined for the production of various grades of steels. And the database is helpful for users to acquire more accurate results of the heat transfer model.

2.1. Research on thermoplastic of steels

Thermoplastic is a key researching content of high-temperature mechanical property of steels. The hot ductility curve of steel should be known in order to make slab avoid "fragile pocket area" during straightening process. Generallyin order to get that useful date, the slab samples will be tested at high temperature by Gleeble tensile testing when the test condition is similar to actual continuous casting process.

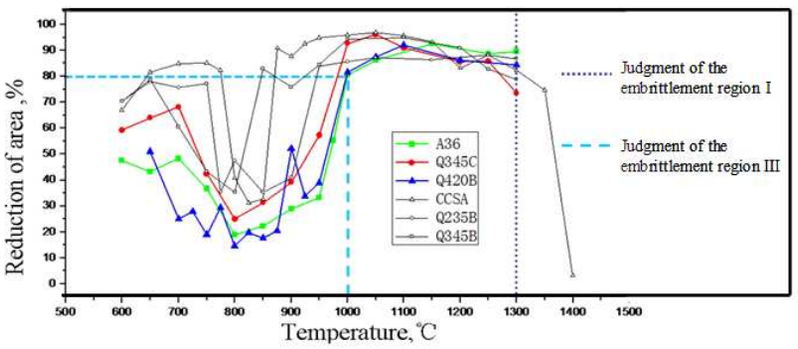

Figure 1. Reduction of area with temperature for some steel grades

According to the experimental results shown in Fig.1, for Nb steel such as A36, it is known that in the embrittlement region◎, temperature range is between melting temperature and 1330 ℃ from the hot ductility curve. Considering the high crack sensitivity of Nb steels, the temperature range of A36 in the embrittlement region ◎ is 600 ℃~ 1000 ℃ when taking the R.A. = 80% as the brittle judgment,in order to ensure the slab has great plasticity. Thus, this brittle judgment can effectively prevent or reduce crack source generation by controlling the slab surface temperature.

It is generally known that the surface temperature fluctuations of slab are impossible to avoid completely during solidification and cooling process. When the temperature fluctuation is large, cracks of some steels such as Nb steel with highly crack sensitivity are easily brought compared with common steels in the process of continuous casting. Therefore, it is proposed especially that the area reduction is more than 80% (the traditional opinion is 60%) for controlling slab surface temperature in each segment exit. Then it should decrease specific water flowrate, cooling intensity and casting speed, in order to effectively prevent crack of Nb steel in the process of continuous casting. Otherwise, it can properly increase withdrawal speed and specific water flowrate for slab casting of steels without Nb to improve the productivity. Generally speaking, the cooling for slabs should avoid the embrittlement region ◎ temperature range as far as possible during straightening process.

As so far, a lot of scholars have tested and researched on hot ductility of many kinds of steels. We can acquire these useful thermoplastic parameters from the literature when needed. Even so, most secondary cooling control systems are difficult to adapt to so many kinds of steels produced by each caster in actual production, due to the difference cooling characteristics of steel grades, especially for new steel production. In author's opinion, the database

http://dx.doi.org/10.5772/51457

of hot ductility should be set up by sorting and summarizing this useful dataFig. 2. At the same time, the database is embedded in the secondary cooling control system in order to acquire the corresponding reference and guidance for different kinds of steels and set suitable target surface temperatures by means of querying data from the database.

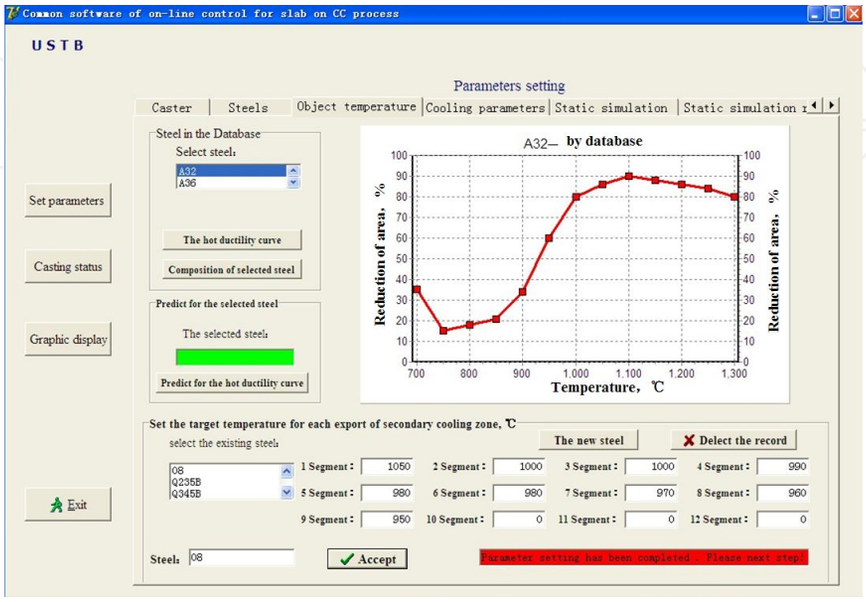

Figure 2. The software interface of the database for hot ductility of steels

The hot ductility of steel is mainly influenced by the chemical composition or technical conditions. Thus, the mathematical model has been established for predicting the reduction of area with chemical composition. The multiple linear regression analysis method has been applied to this model, which was conducted from 24 groups tested data in the similar experiment condition. Moreover, the model considers 12 elements as the independent variables and the reduction of area as the dependent variable.

Gleeble test condition should be similar to deformation and cooling straightening of the industrial operating condition in continuous casting process as far as possible. Mintz's research suggests that the strain rate is 10^{-3} ~ 10^{-4} /s during straightening process. Therefore, this study adopted that strain rate as the rule to select hot ductility of steels from literature..Meanwhile,the cooling rate is 3 ℃ / min.

Besides, because the molybdenum has little impact on thermoplastic of steel and the data of nitrogen content is less than 0.005% basically. Thus, these two elements are ignoredand 12 elements such as C, Si, Mn, P, S, Al, Nb, Ti, V, Ni, Cr, and Cu have been used in regression computation.

Regression methods include the forward method, the backward method and the stepwise regression. The stepwise regression method is adopted extensively, as it can obtain better regression subsets of arguments and a high level of statistical significance. Howeverin this pa-

per, the backward method is selected in order to make the regression reflects the influence of the elements as accurate as possible.

This regression analysis applies SPSS 13.0 software selecting backward method. And the model has been established with comprehensive consideration of three aspects, such as the number of elements, the statistic, the actual impact of the elements on hot ductility and so on. Formula is as (1):

$$\varphi_T = A + \sum \left(B_i \times [i] \right) \tag{1}$$

In formula (1):

φ_T —The reduction of area at temperature T;

A—Real constant;

[i]—The mass percentage of the element i;

Bi—Multiplication coefficient of the element i.

T℃	A	B_C	B_{Si}	B_{Mn}	B_P	B_S
700	114.36	-97.23	-20.46	-13.61	99.33	-734.17
750	148.67	-252.98	8.70	-49.85	478.56	-929.03
800	69.00	-143.38	—	-11.38	—	—
850	11.92	—	—	26.90	477.17	—
900	55.21	—	—	22.69	383.60	-1410.3
950	82.51	—	—	—	—	—
1000	96.00	-114.47	—	—	597.10	—
1050	89.75	-71.84	—	7.86	356.09	—
1100	90.50	-58.72	—	5.80	222.55	—
1150	77.01	33.91	9.63	6.44	—	—
1200	75.26	47.94	15.72	—	—	—
1250	85.22	—	18.30	—	393.09	-775.12
T℃	B_{Al}	B_{Nb}	B_{Ti}	B_V	B_{Ni}	B_{Cr}	B_{Cu}
700	-625.63	-483.49	336.86	—	—	-13.75	—
750	-717.20	—	1609.30	-877.75	140.19	-35.70	-244.36
800	—	-168.32	1134.63	-382.10	57.49	—	-131.32
850	—	-898.73	1712.58	-299.43	—	—	—
900	-222.5	-1070.4	953.0	-576.9	80.36	-38.67	—

http://dx.doi.org/10.5772/51457

T℃	A		B_C	B_{Si}	B_{Mn}	B_P	B_S
950	-251.49	-835.70	1317.37	-360.55	183.88	-41.38	—
1000	—	-447.60	732.06	-161.26	403.80	-88.33	-282.22
1050	—	-441.53	290.78	-91.64	274.55	-68.82	-162.25
1100	114.88	-362.14	—	—	200.44	-44.85	-136.52
1150	77.20	-418.90	405.60	—	76.43	-29.22	—
1200	—	-49.51	—	59.79	-42.96	—	51.38
1250	-143.42	-73.51	—	—	75.94	-35.42	-86.62

Table 1. A, Bi values of formula (2)

The accuracy of regression model needs significant tests. Several important significant test statistics indexes of the regression model are as follows

F: F inspection value; the bigger the F value, the better the significance level is.

R^2Multiple correlation coefficientsreflect regression effect quality: the greater the R^2, the better the regression result is. Generally, R^2 equaling to 0.7 or so can give a positive attitude.

Ra^2: Multiple correlation coefficients after adjustment. Formula is as (2):

$$R_a^2 = 1 - \frac{n-1}{n-p-1}\left(1-R^2\right) \tag{2}$$

Sig: Significant level value; the smaller value, the better result is.

Specific details are shown in Table 2. The significant level value, Sig at different temperatures is all less than 0.1 except for 900 ℃, and it means that the accurate probability of the predicted values is more than 90%. Multiple correlation coefficients, R^2 is more than 0.5 which indicates the better significant of the model.

T℃	Used date	Number of elements	R^2	R^2_a	standard deviations	F	Sig
700	24	9	0.746	0.582	9.9	4.557	0.006
750	24	11	0.860	0.732	12.5	6.700	0.001
800	24	7	0.505	0.289	11.6	2.333	0.076
850	15	5	0.773	0.647	9.1	6.129	0.010
900	24	9	0.526	0.221	18.8	1.725	0.174
950	24	6	0.521	0.352	15.5	3.086	0.031
1000	21	8	0.656	0.426	6.5	2.856	0.050

T℃	Used date	Number of elements	R^2	R^2_a	standard deviations	F	Sig
1050	21	9	0.739	0.526	4.4	3.163	0.028
1100	21	8	0.660	0.433	4.2	2.913	0.047
1150	21	8	0.698	0.497	3.4	3.467	0.026
1200	21	6	0.688	0.554	2.8	5.140	0.006
1250	21	8	0.724	0.540	4.1	3.936	0.017

Table 2. Statistics in significant test of regression model

In order to prove the accuracy of the hot ductility prediction model, the tested data selected from literatures, which is outside the regression analysis samples data, has been compared with the prediction model for pipeline steels and weathering steels.

The chemical composition of two steel grades is shown as Table 3. Test conditions for the strain rate is 1.0×10^{-3} / sand the cooling rate is 3 ℃ / min.

type of steel	C	Si	Mn	P	S	Al	Nb	Ti	V	Ni	Cr	Cu
weathering steel	0.094	0.295	0.4	0.076	0.005	0.033	—	—	—	0.22	0.53	0.29
Pipeline steel	0.054	0.224	1.6	0.008	0.002	0.037	0.054	0.013	0.042	0.17	—	0.18

Table 3. The chemical composition of pipeline steel and weathering steel

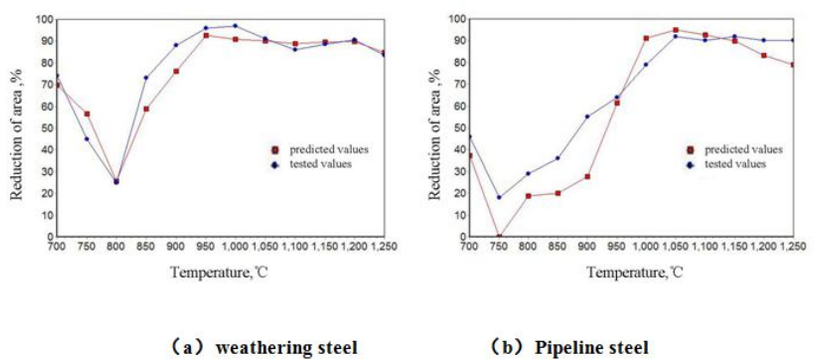

Figure 3. Comparison of hot ductility between predicted values and tested values

The curve of predicted values is very close to tested values and they have the same tendency by comparison from the Fig.3. It should be aware that the predicted values will be difficult in exact conformity with the tested values due to test conditions and test errors. Therefore, it shows that prediction model of thermoplastic established in this paper has a better practica-

http://dx.doi.org/10.5772/51457

bility. Even so, the model has some limitations because of less regression sample data of only 24 groups. But with more studies on hot ductility, the model will evolve further.

2.2. Formulae for thermal physical parameters

The thermophysical property parameters of steel such as density, conductivity coefficient, specific heat capacity, latent heat, liquidus temperature, and solidus temperature are essential for calculating the heat transfer model. Although these parameters can only be acquired accurately by tests, the thermophysical properties of a new steel grade can also be approximately calculated from the chemical composition with the requirements of more steel grades to cast.

2.2.1. Liquidus temperature

The liquidus temperature of steel plays a very important role in metallurgical production and related scientific research. The lowest superheat may be achieved during the process of continuous casting if an accurate liquidus temperature of steel is obtained. This is described as it is useful to acquire a fine grain structure and higher quality of slab for steel plants. The accurate liquidus temperature of steel is also required for scientific investigation of solidification processes of molten steel by numerical simulation. Research shows that the main reason why the liquidus temperature of steel is lower than the melting point of pure iron is the presence of impurities and alloying elements. Generally speaking, there are two ways to obtain the liquidus temperature of steel for the research: firstly, as a standard method for determining transformation temperature of materials, a differential thermal analysis (DTA) measurements is conducted, and a number of studies have used DTA for the determination of liquidus temperature; secondly, the more common method, is to select the appropriate model according to the different kinds of steel. On the basis of the analysis of Fe-i binary phase diagram, a new calculation model for liquidus temperature of steel is established in this study.

The different effects of 11 elements (C, Si, Mn, P, S, Ca, Nb, Ni, Cu, Mo,Cr) on the melting point of pure iron were investigated and 11 groups of discrete data (A_C, A_{Si}... A_{Cr})that isthe value of liquidus temperature was decreased or increased together with the content of element i increase (or decrease) by 0.1% mass fraction in Fe-i binary phase diagramwere obtained. Then, each group data was fitted to obtain the mathematical formula (ΔT_{lc}, ΔT_{lsi}, ...ΔT_{lMo}). Finally, the model of steel liquidus temperature can be establishedintroducing the mathematical formulae of each element into the Eq.(3).The calculation model for steel liquidus temperature developed in this study is as follows

$$T_l = T_0 - \sum \left(\frac{\partial T_l}{\partial C_i} \times [\%C_i] \right) \tag{3}$$

Where

T_l —Liquidus temperature of steel, ℃;

T_0—Melting point of pure iron, ℃, the general value range is 1534~1539℃, and T_0 is 1538℃ in this study;

$\partial T_l/\partial C_i$—The changing rate of liquid isotherm to the content of element i on Fe-i binary phase diagram;

[%C_i]—The percentage content of element i.

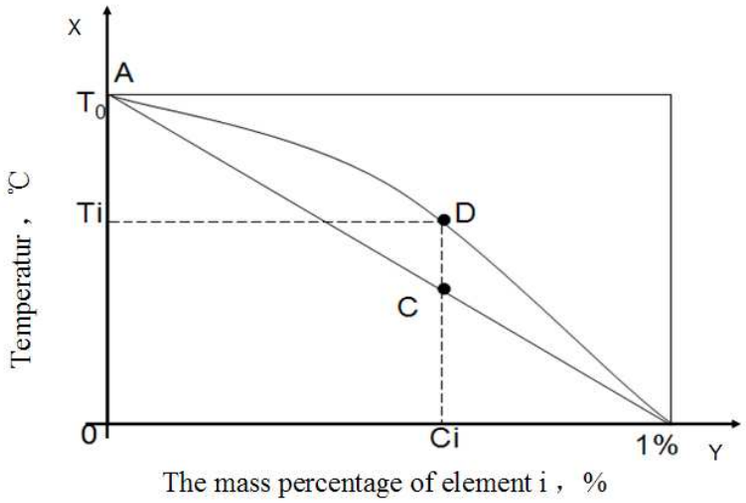

Figure 4. The influence of element i on the liquidus temperature

In Fig. 4, the X axis represents the mass percentage of element i and the Y axis represents temperature. The curve ADB is the change in the actual liquidus temperature with the content of element I; however, most research on liquidus temperature assumed that the influence of each element on reduction value of the melting point is kept linear relation (shown as the straight-line segment AB). Therefore, the calculation is easy to result in deviation. For instance, when the content of the element i is C, the liquidus temperature is the value corresponding to C (where point C corresponds to the liquidus temperature according to traditional models), however the actual liquidus temperature is T_i (corresponding to point D). Therefore, the deviation is the line segment CD. As a result, the traditional calculation model for liquidus temperature of steel is likely to have a large error when steel has many elements.

Owing to drawbacks of the general models for liquidus temperature calculation, a new model is needed. After differentiated the Fe-i binary phase diagram, new temperature coefficients of each element in the molten steel is obtained, a new calculation model for liquidus temperature is established. The margin of error with the use of this universal model is likely to be less than that with traditional models. All the alloying elements of steel or cast iron influence the liquidus temperature; however, the element which has the greatest effect is

http://dx.doi.org/10.5772/51457

carbon. Considering an example of the phase diagram of Fe-C and amplifying the part of interest will help explain this.

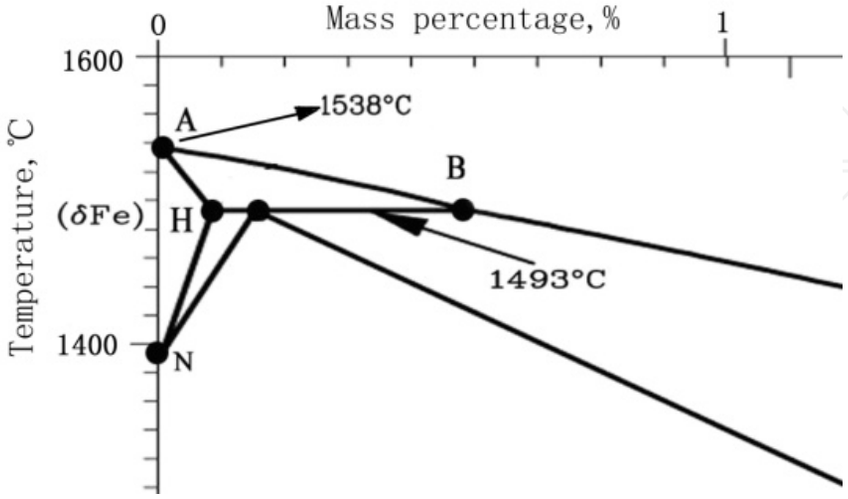

Figure 5. Partial Fe-C binary equilibrium phase diagram enlarged

Processing of the curve AB in Fig.5 by Photoshop software shows the influence of carbon content on the liquidus temperature (Table 4).

CContent, %	0.01	0.02	0.03	0.04	0.05	0.06	0.07	0.08	0.09
$\triangle T_l$,℃	2.00	2.50	3.00	3.40	4.40	4.90	5.70	6.10	6.70

Table 4. Impact of carbon content on the liquidus temperature

The data in Table 4 are fitted with the least square methodand the calculation formula for the influence of carbon content on steel liquidus is established and expressed as:

$$\Delta T_k = 32.15[\%C]^2 + 62.645[\%C] - 0.8814 \tag{4}$$

$$T_l = 1538 - \begin{pmatrix} 31.15[\%C]^2 + 62.645[\%C] + 0.609[\%Si]^2 + 2.0678[\%Si] - 0.0674[\%Mn]^2 \\ +5.3464[\%Mn] + 20[\%P]^2 + 9[\%P] - 1.7724[\%S]^2 + 24.775[\%S] + 1.1159[\%Nb]^2 \\ +5.3326[\%Nb] - 0.0758[\%Ca]^2 + 3.1313[\%Ca] + 0.0379[\%Ni]^2 + 5.2917[\%Ni] \\ +0.6818[\%Cu]^2 + 2.5955[\%Cu] + 0.0214[\%Mo]^2 + 3.2214[\%Mo] + 0.0359[\%Cr]^2 \\ +1.1402[\%Cr] + 10.797 \end{pmatrix} \tag{5}$$

In the same way, for Si, Mn, P, S and other elements, their binary phase diagrams are processed, and different formular for each elements influence on the steel liquidus are obtained. Finally, a new model for calculating steel liquidus temperature is set up by synthesizing, which is verified with some testing liquidus temperature of steel, shown as Eq.(5).

It has been proved that errors between liquidus formula (5) with others are all less than 4 ℃.

2.2.2. Thermal conductivity coefficient

Thermal conductivity coefficient of steel solid-phase is relevant to temperature and elements. For carbon steels and stainless steels, the expression is shown as Eq. (6). Moreover, due to the great influence of liquid convection in liquid core, the equivalent thermal conductivity coefficient is used for liquid-phase.

$$\begin{aligned}\lambda^S &= 20.76 - 0.009T - 3.2627[C] + \begin{pmatrix} 0.0124 - 2.204\times10^{-4}T \\ +1.078\times10^{-7}T^2 + 7.822\times10^{-4}[Cr] - 1.741\times10^{-7}T\cdot[Cr] \end{pmatrix}[Cr] \\ &+ \begin{pmatrix} -0.5860 + 8.354\times10^{-4}T - 1.368\times10^{-7}T^2 + 0.01067[Ni] \\ -1.504\times10^{-5}T\cdot[Ni] \end{pmatrix}[Ni] - 0.7598[Si] - 0.1432[Mn] \\ &-0.2222[Mo]\end{aligned} \tag{6}$$

$$\lambda^L = m\lambda^S \tag{7}$$

$$\lambda^{SL} = \lambda^S f_S(T) + \lambda^L\left(1 - f_S(T)\right) \tag{8}$$

Where,

$\lambda^L\lambda^S\lambda^{SL}$— the conductivity coefficient of liquid phase, solid phase and mush zoon respectivelyW/(m ℃)

T —Temperature℃

[i] —The mass percentage of the element i%

$f_S(T)$—Solid fraction

m —Equivalent coefficient.

2.2.3. Density

The density with high temperature of carbon steels is relevant to the carbon content and temperature. Its solid, liquid density can be used formula (9), (10) to calculate.

http://dx.doi.org/10.5772/51457

$$\rho_S = \frac{100\left(8245.2 - 0.51\left(T + 273\right)\right)}{\left(100 - \left[C\right]\left(1 + 0.008\right)\left[C\right]\right)^3} \tag{9}$$

$$\rho_l = 7100 - 73\left[C\right] - \left(0.8 - 0.09\left[C\right]\right)\left(1550 - T\right) \tag{10}$$

But for stainless steels, it is strongly related to Cr, Ni, Mo, Mn, Si and other major elements, the expression is shown as formula (11), (12)

$$\rho_s = \begin{pmatrix} 79.6\%\left[Fe\right] + 78.3\%\left[Cr\right] + 85.4\%\left[Ni\right] + 76.9\%\left[Mn\right] + \\ 60.2\%\left[Mo\right] + 47.1\%\left[Si\right] \end{pmatrix} - 0.5\left(T - 25\right) \tag{11}$$

$$\rho_l = \begin{pmatrix} 69.4\%\left[Fe\right] + 66.3\%\left[Cr\right] + 71.4\%\left[Ni\right] + 57.2\%\left[Mn\right] + \\ 51.5\%\left[Mo\right] + 49.3\%\left[Si\right] \end{pmatrix} - 0.86\left(T - 1550\right) \tag{12}$$

$$\rho_{sl} = \rho_s f_S\left(T\right) + \rho_l\left(1 - f_S\left(T\right)\right) \tag{13}$$

Where

$\varrho_s\varrho_l\varrho_{sl}$—The density of solid phase, liquid phase and mush zoon respectivelykg/m^3

T—Temperature℃

[i] —The mass percentage of the element i%

f_S(T) —Solid fraction.

Moreover, formulae for specific heat and latent heat have been described in many research literatures. They will not be mentioned in this chapter.

Because thermal physical parameters have an important influence on the accuracy for the heat transfer calculation model, the database of thermal physical parameters, such as liquidus temperature, conductivity coefficient, density and so on, has been established by summarizing, which can provide accuracy “basic parameters” for the "targeted” solidification and heat transfer numerical model.

3. Control models for secondary cooling in continuous casting process

Secondary cooling control, which is a key technology in the continuous casting process, not only determines the productivity of a caster, but also significantly influences the quality of

the slab. Currently, nearly all secondary cooling control systems are based on a heat transfer model of solidification during continuous casting, which makes the control process more quantitative. At present, there are several popular control models for secondary cooling in continuous casting, such as the parameter control model, effective-speed control model, online thermal model, and models that are combinations of these. These control models have their respective advantages and meet the modern requirements of the continuous casting process on the whole. Even so the mathematical heat transfer model of solidification is an important base for secondary cooling control, so authors will briefly introduce it before expounding the control models of continuous casting.

3.1. Heat transfer model

The mathematical heat transfer model of solidification during continuous casting is composed of heat conduction equations, initial conditions, and boundary conditions. The heat conduction along a strand is usually neglected. The unsteady two-dimensional equation of heat transfer is shown as below:

$$\rho c_p \frac{\partial T}{\partial \tau} = \frac{\partial}{\partial x}\left(\lambda \frac{\partial T}{\partial x}\right) + \frac{\partial}{\partial y}\left(\lambda \frac{\partial T}{\partial y}\right) + q_v \tag{14}$$

Where, q_v is internal heat source, which is latent heat (J kg^{-1}) here and can be equivalent to the equivalent specific heat capacity or effective thermal enthalpy to simplify the conduction equation. The heat transfer model is the basis for the quantitative method of controlling the secondary cooling water, and many models of secondary cooling control have been developed. Some popular control models are reviewed in this chapter, as follows.

3.2. Control models for secondary cooling

3.2.1. Parameter control method

The parameter control method requires determination of the target surface temperature curves for different steel grades; calculation of the control parameters A_i, B_i, and C_i for every secondary cooling zone such that the strand surface temperature coincides with the target surface temperature; and building a mathematical model as in equation (15).

$$Q_i = A_i V^2 + B_i V + C_i \tag{15}$$

With the wide use of continuous temperature measurements of molten steel in the tundish and growing research on the influence of the temperature of secondary cooling water on slab cooling, the superheat and the temperature of the secondary cooling water have been considered to be the important factors for controlling the surface temperature of the slab. The secondary cooling water flow rate needs to be adjusted accord-

http://dx.doi.org/10.5772/51457

ing to these two factors, so equation (15) can be modified and improved, whereby equation (16) is presented as follows:

$$Q_i = A_i V^2 + B_i V + C_i + D_i \Delta T + F_i \tag{16}$$

Where, D_i is the adjusting parameter for the water flow rate based on superheat, and F_i is the adjusting parameter of water flow rate based on the temperature of the secondary cooling water, which changes with the season.

The water flow rate in the parameter control method changes with the variation of casting speed continuously, and are controlled according to the theory of the solidification of the slab and the practical conditions. The control pattern can be run in an automatic, manual, or semi-automatic way. Indeed, the parameter control method requires little investment but has strong applicability, and so is still widely applied in steel plants. However, the control method shows an apparent disadvantage: the parameter control method cannot keep the stability of the slab surface temperature in the unsteady casting state, such as in the case of a change in the submerged entry nozzle and the hot exchange of the tundishes. Therefore, an improved control method called the "effective speed" method has been developed based on the parameter control method.

3.2.2. Effective speed control method

The effective speed control method is derived from the residence time control method of slabs. As shown in Fig.6 (the calculating model of residence time of a slab), the slab is divided into a number of small slices, each slice is pulled forward at the casting speed of the slab, and new slices are generated at regular intervals. The residence time can be regarded as approximately the same for a slice. Once the slice is pulled out of the end of the secondary cooling zone, it is no longer tracked, and is deleted from the computer memory. The data for each slice are updated at regular intervals; this includes the distance from the meniscus to the position of the slice and its running time in the caster, which is called the "residence time."

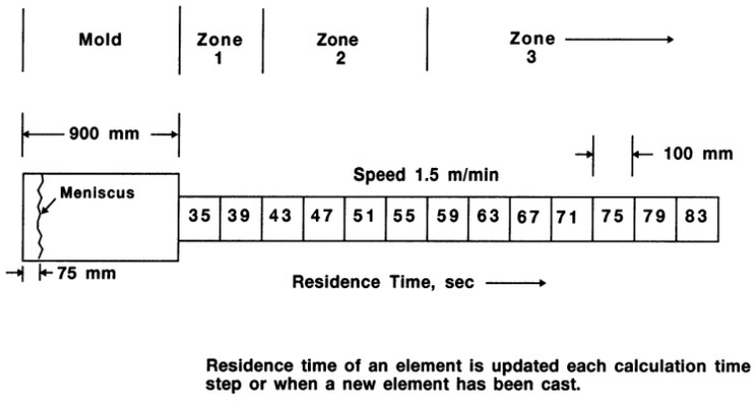

Figure 6. The calculation model for the residence time of a slab

The relationship between the residence time and the water flow rate can be converted into the relationship between the average speed and water flow rate. The average speed of one cooling zone can be calculated from equation (17):

$$V_{ai} = \frac{S_i}{\frac{1}{n_i} \cdot \sum_{j=1}^{n_i} t_{rij}} \tag{17}$$

It has been shown that a modified effective speed based on the average speed can be used to reduce surface temperature fluctuations and improve the safety of continuous casting operations. Effective speed can be calculated by equation (18):

$$V_{ei} = \varepsilon_i V_{ai} + (1 - \varepsilon_i) V \tag{18}$$

Where, ε_i is the weighting coefficient, which is between 0 and 1, and depends on the distance from the center of the zone to the meniscus: i.e., the longer the distance, the higher is the value.

The equation of the effective speed control method is constructed by replacing the real-time speed in equation (15) with the effective speed, shown as below:

$$Q_i = A_i V_{ei}^{\ 2} + B_i V_{ei} + C_i \tag{19}$$

Fig.7 and Fig.8 show the fluctuation of the slab surface temperature calculated by the computer simulation using the parameters control model and the effective speed control model, both with the same speed conditions. Compared with the parameters control model, the effective speed control model can keep the surface temperature smoother in the unsteady casting state of speed fluctuations, such as the change of the submerged entry nozzle.

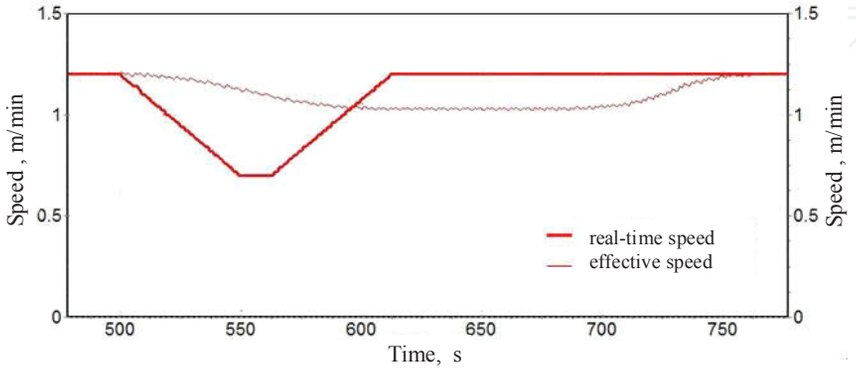

Figure 7. Fluctuation of the effective speed of the third zone due to a fluctuation in the casting speed

http://dx.doi.org/10.5772/51457

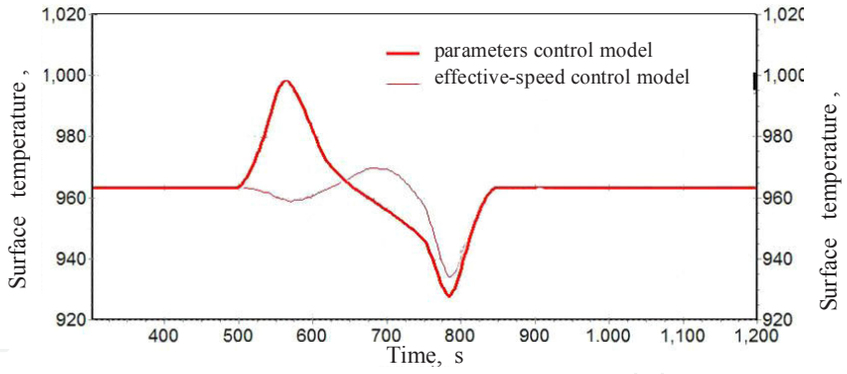

Figure 8. Comparison of the surface temperature fluctuations at the end of the third cooling zone (4.2 m from the mold meniscus) for the two control methods(Section is 220 mm×1600 mm, casting temperature is 1818 K, peritectic steel)

The parameter control method and the effective speed control method are both based on an off-line thermal model. With advances in computational technology and the reduction of computational costs, online calculation of temperature profiles is no longer a problem. The online thermal model control method is based on an online simulation model of heat transfer and controls the water flow rate of secondary cooling zones through real-time calculation of the slab temperature profile.

3.2.3. Online thermal model control method

The online thermal model control method can be described as follows. The online simulation model of heat transfer calculates the real-time temperature profile of the slab at certain intervals, and the water flow rate of the secondary cooling zones is controlled by the deviational value of the target temperature and calculated temperature.

The water flow rate control relies only on the feedback of the surface temperature calculated by the online thermal model and has a hysteresis quality. The stability of the control system is poor, because the control system has a strong dependency on the accuracy of the calculated surface temperature. Therefore, the online thermal model control method needs to be combined with other feed-forward control methods, for example, a combination of the online thermal model with the effective speed control method, shown as equation (20). In this control method, the surface temperature is controlled through setting the basic water flow rate with effective-speed and fine-tuning it with the deviational value between the target temperature and the calculated temperature to further reduce this deviation.

$$Q_i = f_1(V_i) + f_2(\Delta T_{fi}) \tag{20}$$

Where, $f_1(V_{ei})$ is the water flow rate calculated using the effective speed model, and $f_2(\Delta T_{fi})$ is the water flow rate calculated based on the deviation value between the target temperature and the calculated temperature using the online thermal model.

This control method is characterized by good stability and accuracy and no delays, thus it enables the surface temperature to be controlled around the target values. Fig.9 shows the fluctuations of the measured surface temperature at a position 5.0 m from the meniscus with fluctuations in the casting speed in a continuous casting process. It can be seen in the figure that the surface temperature of the slab is controlled around 920°C despite strong fluctuations of the casting speed.

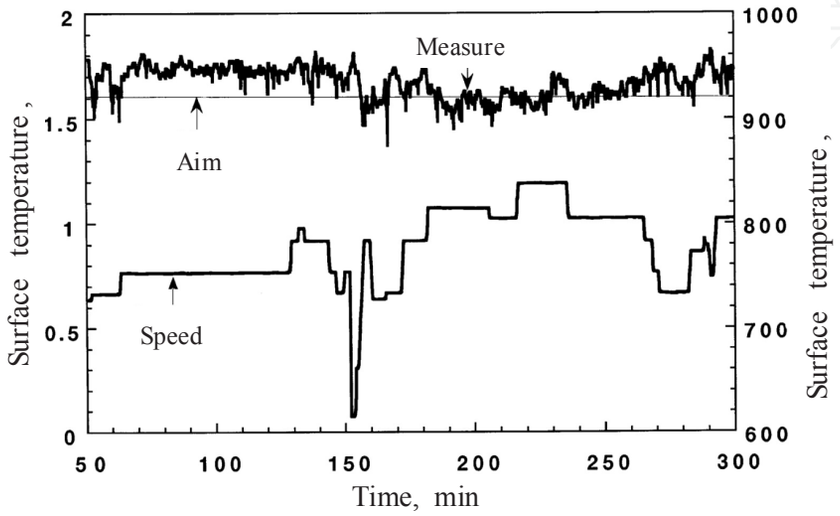

Figure 9. Measured fluctuations of the surface temperature at a position 5.0 m from the meniscus

The online thermal model can calculate the real-time surface temperature of a slab, but due to the inevitable deviation between the calculated temperature and the actual temperature, the actual surface temperature can only be obtained by measurement. Therefore, while a system of water flow rate control that relies only on the feedback of the measured surface temperature is not commonly adopted, a thermometer combined with an online thermal model can be applied as one of the main tools of secondary cooling control. In this case, the feedback value is not directly used to control the water flow rate, but to dynamically adjust the parameter A in equation (9), which reflects the relationship between the heat transfer coefficient and water flow rate, and to eliminate the temperature error – the difference between the calculated temperature and the measured temperature. The thermometer does not need to be working continuously, rather, the online thermal model can be corrected with temperature measurements at certain intervals; thus the expenditure of thermometers is improved, and the accuracy of the online model and precision of the secondary cooling control is ensured.

3.2.4. Synthetical model dynamic control method based on online temperature measurement

In order to build a new secondary cooling control model that integrates the advantages of the control methods mentioned above, the concept of effective superheat is put forward, and the synthetical model dynamic control method based on online temperature measurement is established in this study.

http://dx.doi.org/10.5772/51457

Effective superheat is obtained by modifying the average superheat. In the parameter control method, the water flow rate compensation according to superheat is based on the real-time superheat, and this control model can meet the control requirements of the surface temperature only in the case of small fluctuations in the casting temperature. However, if the fluctuations are large, the surface temperature of the slab will not be controlled. In order to achieve accurate water flow rate compensation according to superheat, the initial superheat in the meniscus of the slab should be obtained, and thus the average superheat needs to be applied. In the residence time model of the slab (shown in Fig.6), the computer not only calculates the residence time of each slice, but also stores the data of the initial superheat of each slice when it is generated. The average superheat $\triangle T_a$ of one zone is the average value of the initial superheats of all the slices in this cooling zone. The average superheat represents the initial superheat of the slab in a cooling zone, but there are shortcomings in applying this method. Because of the upper and lower convection from the liquid core, the temperature of the liquid steel in the mold influences the temperature profile of a slab with a liquid pool. Furthermore, the shorter the distance of a cooling zone from the mold, the stronger is this effect. In addition, the water flow rate of the cooling zone closer to the mold cannot be adjusted in time when using the average superheat, thereby a breakout may happen if the casting temperature suddenly rises in the continuous casting process. Therefore, with regards to the effective speed, the average superheat should be corrected, and the effective superheat $\triangle T_e$, derived, as shown in equation (21):

$$\Delta T_{ei} = \lambda_i \Delta T_{ai} + (1 - \lambda_i) \Delta T \tag{21}$$

Where,ΔT_{ei} is the effective superheat of zone i ℃;ΔT_{ai}, average superheat;ΔT, real time superheat; andλ_i the weighting coefficient, which ranges from 0 to 1. The weighting coefficient depends on the distance from the cooling zone to the meniscus: the further the distance, the greater is the value. The value is 1 at the cooling zone of the solidification endpoint.

Fig.10 and Fig.11 show the surface temperature simulated fluctuations of a slab with conditions of no water flow rate compensation according to superheat, water flow rate compensation according to real time superheat and water flow rate compensation according to effective superheat under the same casting temperature conditions. It is evident that when the superheat rises sharply when the casting speed is stable, the surface temperature is not well controlled with no water flow rate compensation according to superheat. When the casting temperature rises, the surface temperature increases. Moreover, with water flow rate compensation according to real time superheat, the surface temperature undergoes large fluctuations although it can return to the temperatures close to those before the casting temperature rise. In the mode of water distribution based on the water flow rate compensation according to effective superheat, not only does the surface temperature almost return to what it was before the increase of the casting temperature, the temperature fluctuations are also much smaller, showing better control of the surface temperature.

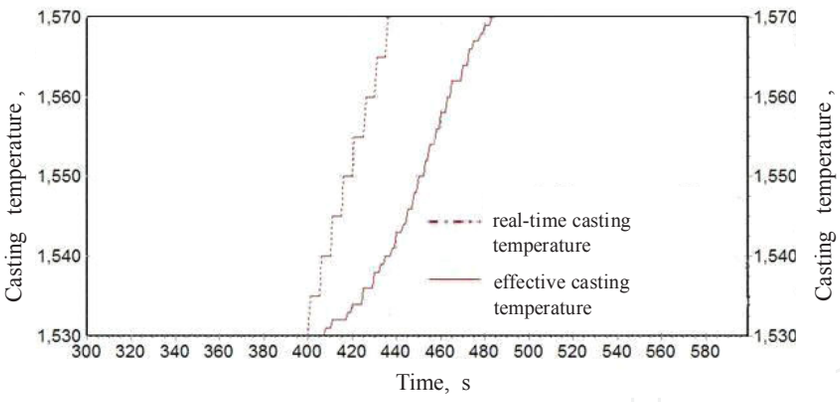

Figure 10. Effective casting temperature fluctuation in the foot-rollers cooling zone with a fluctuation of the pouring temperature

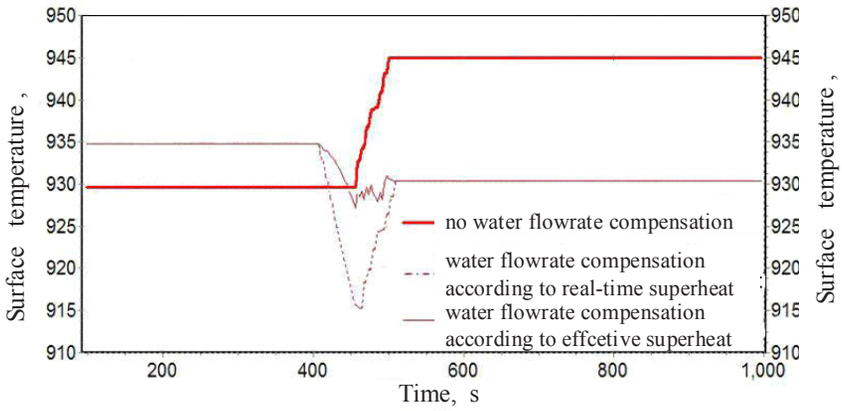

Figure 11. Comparison of the surface temperature fluctuations at the end of the foot-rollers cooling zone(1.2 m from the meniscus) under three modes of water flow rate compensation(Section is 220 mm × 1600 mm, withdraw speed is 1.0 m/min, peritectic steel)

The various control models mentioned above have different characteristics. By integrating them, a new synthesized secondary cooling control method called "synthetical model dynamic control method based on online temperature measurement" can be deduced, as shown in equation (22):

$$Q_i = f_1(V_{ei}) + f_2(\Delta T_{ei}) + f_3(\Delta T_{fl}) \tag{22}$$

Where $f_1(V_{ei})$ is the water flow rate determined by effective speed; $f_2(\Delta T_{ei})$, the water flow rate determined by effective superheat; and $f_3(\Delta T_{fi})$, the water flow rate determined by the deviation value between the target surface temperature and the calculated surface temperature.

http://dx.doi.org/10.5772/51457

In this control model, the surface temperature is controlled through setting the feed-forward water flow rate with effective speed and effective superheat, and carefully adjusting it with the deviational values of the target temperature, using the adjusting pattern of the PID control algorithm. In addition, this control system with an online thermometer can modify the online thermal model with time when casting conditions change. The control logic is shown in Fig.12.

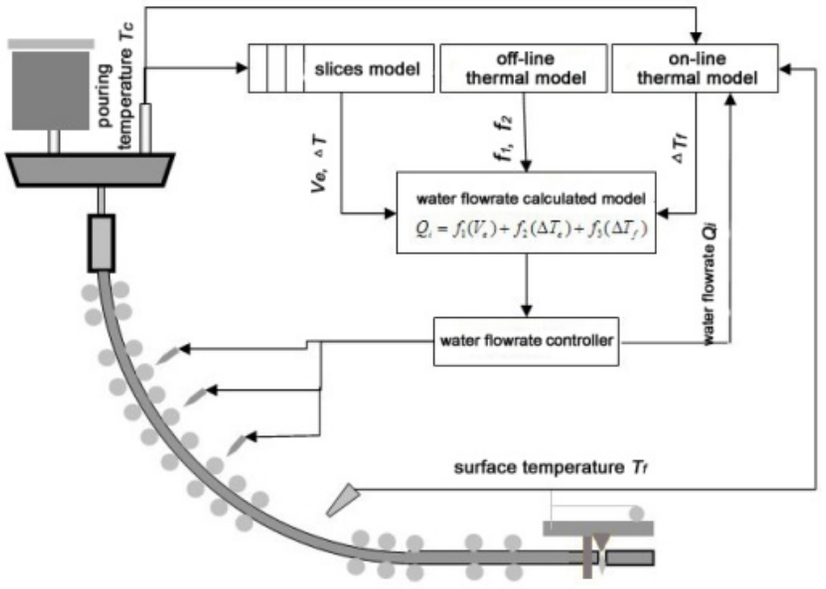

Figure 12. Control logic of synthetical model dynamic control method based on online temperature measurement

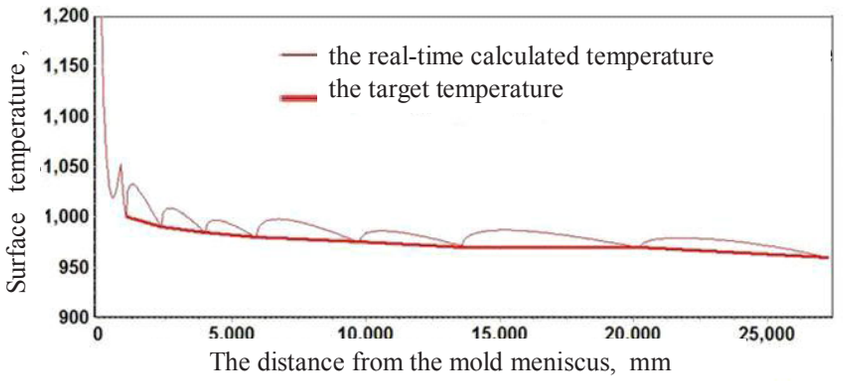

Figure 13. Comparison of real-time calculated surface temperature and the target surface temperature

Fig.13 shows the center surface temperature profile of peritectic steel whose cross section is 1600 mm × 220 mm at a withdraw speed of 1.2 m/min, and superheat 1818 K.

It reveals that in this control method, the surface temperature is well controlled around the target temperature.

This study summarizes the principles and characteristics of several popular models of secondary cooling control and furthermore, puts forward the concept of the effective superheat and an improved model called "synthetical model dynamic control based on online temperature measurement." This new control method demonstrates good control of the slab's surface temperature. As the requirements on slab quality continue to rise, the secondary cooling control system will play an important role in the casting process. Many new technologies such as dynamic soft reduction, the quality of online evaluation and forecasting and the direct rolling process, are based on an advanced control system of secondary cooling as the pre-condition. A secondary cooling control system not only needs to ensure a smooth slab surface temperature distribution, but also provides real-time information of the slab's temperature profile and the end of the liquid pool. In addition, the rapid development of information technology will also push the secondary cooling control to the level of intelligent and full automation. From work presented here, we can conclude that the subject of secondary cooling control systems needs further research and development from the following aspects:

1. The operation conditions in special periods, such as at the start or end of the casting or at the hot exchange of the tundishes, should be taken into account in the control model, in order to guarantee the slab quality at these points and improve the recovery ratio of metal.
2. Durable, accurate, online surface temperature measuring sensors should be developed to provide continuous, accurate feedback data for the secondary cooling control system, and achieve dynamically precise cooling control of the slab.
3. For further improvement of the simulation models for continuous casting processes, thermal-mechanical coupling should be introduced into the online calculation model, so that the models can not only provide real-time temperature profiles, but also provide the stress field, shell shrinkage, and a function for online crack forecasting.

4. Influence of nozzle layouts on the secondary cooling effect of slabs

The effect of spray water on heat transfer of slab surface depends on the performance of the nozzle. Therefore, in order to analyze cold characteristics of the nozzle, improve the slab quality by the optimization of secondary cooling system, and improve the continuous casting productivity, a series of experiments should be carried out.

Taking the CCM2 at the No.3 steelmaking plant of Hansteel for example, flat type air mist nozzles are used in the segments, with three nozzles arranged in each row. The distance between adjacent nozzles is 450mm, and the height from the slab surface to a nozzle is 380mm. As the spraying angle is 110°the water sprayed from the nozzles appears to be triple overlaid on the center surface of the slab, which causes water accumulation in the region. In ad-

http://dx.doi.org/10.5772/51457

dition, the presence of excessive water is at the corner region. Uneven cooling along the width direction of the slab can easily lead to slab cracks and other defects.

Figure 14. Experimental device of cold characteristics test for cooling nozzles

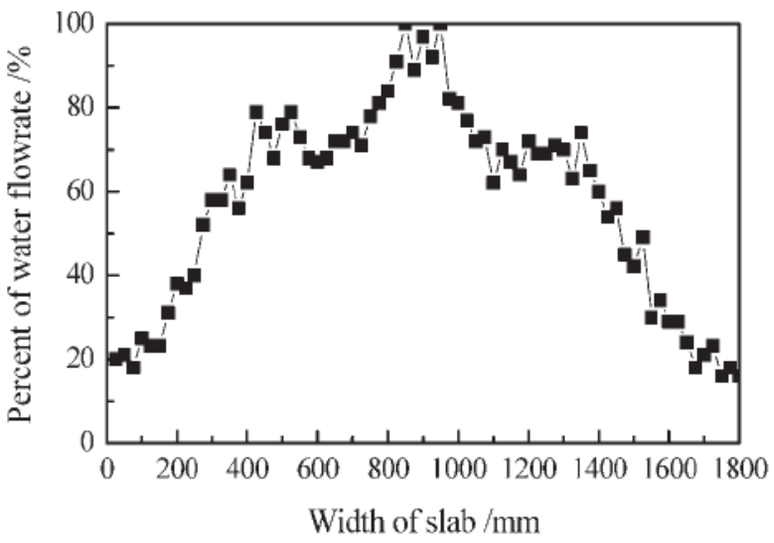

Figure 15. Water distribution along slab width direction before optimisation(water pressure, 0.2 MPa; air pressure, 0.2 MPa)

4.1. Influence of spray water distribute on secondary cooling effect of slabs

Based on the mathematical model, the stress and strain fields of the slab were also studied under specific casting conditions using the finite element software ANSYS. Considering the symmetry of a slab cross-section, half of the slab cross-section was taken as

the research object. Under the current arrangement of nozzles, the distribution of water flowrate in the slab width direction was measured as shown in Fig.15. Before optimization at the straightening zone, the temperature profile of the slab surface in the slab width direction was as shown in Fig.16.

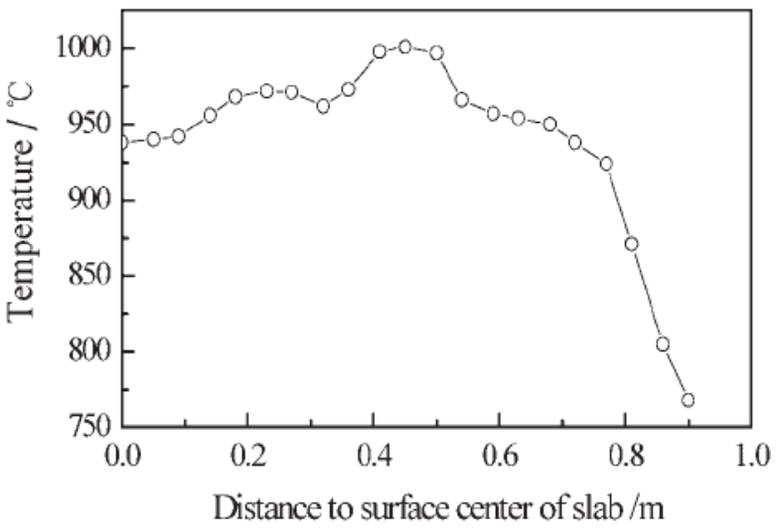

Figure 16. Temperature behavior of slab surface in slab width direction before optimization(Half section, casting speed, 0.9 m min^{-1}; superheat, 27℃, 18 m below meniscus)

As can be seen from the Fig.16, due to the poor spray cooling pattern, there is an uneven surface temperature distribution in the slab width direction. The temperature at the surface center of slab is only 938℃, while the highest temperature value of the slab surface is 1001℃, which is near the quarter of the whole slab width. Moreover, the lowest temperature of 768℃ is at the slab corner.

This chapter analyses fully the stress field of the slab in the straightening region, between 15.86 and 20.24m below the meniscus. Because the slab is not fully solidified when the slab enters into the straightening zone, the temperature of central region of slab is still above the liquidus temperature. In order to simplify the model, the equivalent stress analysis is only focused on the solidified shell. The temperature field before optimization is set as the initial condition; meanwhile, corresponding ferrostatic pressure is imposed on the solidifying front of the slab for stress analysis. The ferrostatic pressure can be expressed as equation (23).

$$\Delta P = \rho g H \tag{23}$$

The equivalent stress field of the slab is simulated under the action of the straightening roller along the casting direction, as shown in Fig. 17.

http://dx.doi.org/10.5772/51457

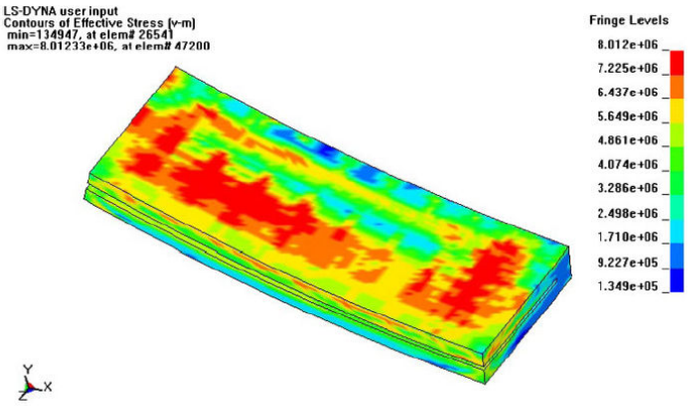

Figure 17. Equivalent stress field of slab at straightening segment before optimization(steel grade, Q420B; section, 1800×220 mm; casting speed, 0.9 m min21; superheat, 27℃)

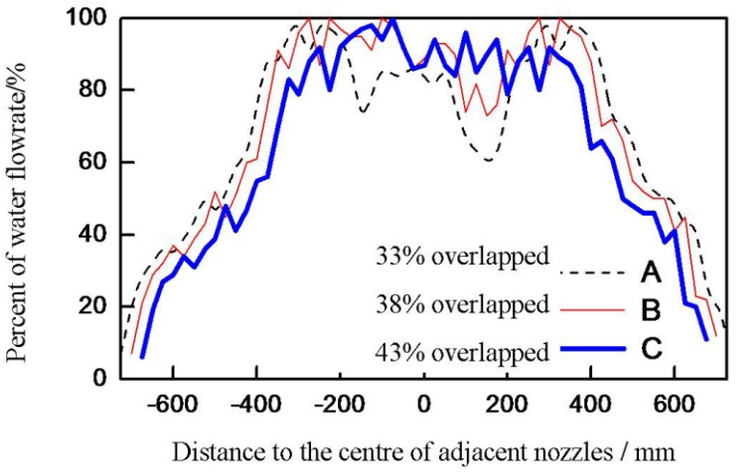

Figure 18. Water distribution with two nozzles along the slab width direction water flowrate :3.9 L min^{-1};injection height :300mm

The figure shows clearly that the maximum equivalent stress on the slab reaches 8.012 MPa in the straightening zone under the direction of the slab, which results in a high temperature gradient in the slab. Hence, the corresponding equivalent stresses in these regions are larger than those of the other regions, which can generate easily slab defects. Uneven cooling usually appears in the width direction of a slab because of its large width. As an additional factor, the heat transfer occurs on two directions at the corner of a slab. Thus, the design scheme for a secondary cooling system should obey the rules of a homogeneous cooling distribution in the width direction and a gradual decrease in the cooling range along the width direction from the top to bottom of the caster; this should prevent defects caused by undercooling in the corner region of the slab. Based on the temperature and stress analysis of the slab, combined with cold test performance data of the nozzles, a new scheme for the secondary cooling system is proposed.

4.2. Influence of nozzle layouts on the spray water distribution

The principle of nozzles arrangement is to make spray water distribute evenly in the width direction of slab surface. Through a series of test for combined nozzles on the platform of nozzle automatic testing, the relationship between spraying overlap degree of adjacent nozzles and the uniformity of water distribution in slab width direction is analyzed from three aspects such as nozzle flow rate, injection height, water pressure and air pressure.

As can be seen from Fig.18water distribution of scheme C whose spray overlap degree of adjacent nozzles is 43%, is more even in slab width direction when the water flow rate is 3.9 L min^{-1} and injection height is 300 mm.

After the optimization, the distribution of the water flowrate in the slab width direction is improved significantly, as shown in Fig. 19.

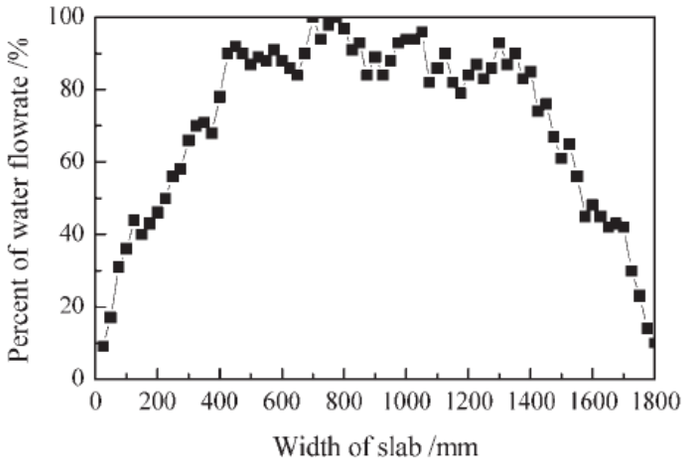

Figure 19. Water distribution along slab width direction after optimization(Water pressure: 0.2 MPa, air pressure: 0.2 MPa)

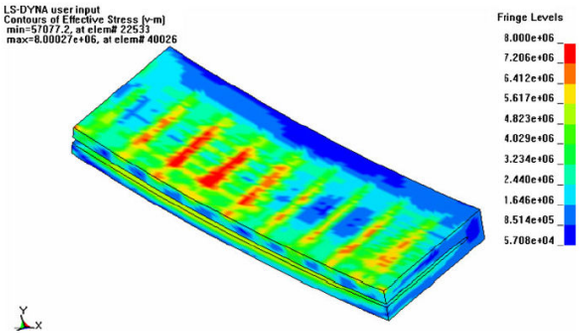

Figure 20. Equivalent stress field of slab at straightening segment after optimization (Steel grade, Q420B; section, 1800×220 mm; casting speed, 0.9 m min^{-1}; superheat, 27℃)

http://dx.doi.org/10.5772/51457

On the basis of the optimization of the temperature field, the stress field of a slab at the straightening zone was analyzed. The simulation results for the equivalent stress field in the straightening zone of the slab after optimization are shown in Fig. 20.

Comparison of Figs. 17and 20 shows that although the maximum values of equivalent stress decrease from 8.012 to 8.000 MPa after optimization (only reduced by 0.012 MPa), the stress concentration has almost disappeared. The larger stresses shown in Fig. 13 exist only where the slab and the rollers are in contact because of the ferrostatic pressure of the molten steel. However, a wide range of slab surface was under the state of large equivalent stress before optimization, which was harmful to the surface quality of the slab. In the software simulation, the temperature and stress fields were both greatly improved, which was useful to improve the quality of the slab.

Through the experimental studies of the flat type nozzle, nozzles arrangements have a major impact on spray water distribution, not only due to the distance of adjacent nozzles and the height of nozzles, but also due to the degree of flat type nozzle bias. As is shown in Fig.21, if the water is sprayed in a straight line at each row with same nozzle type, water pressure and air pressure, and so on.

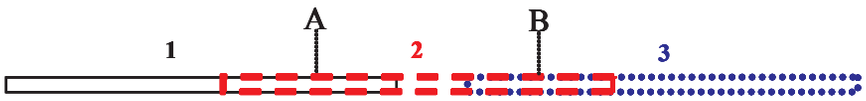

Figure 21. Nozzles distributed in a straight lineA,B is the center of adjacent two nozzles,1,2,3 is spray area for three flat type nozzles respectively)

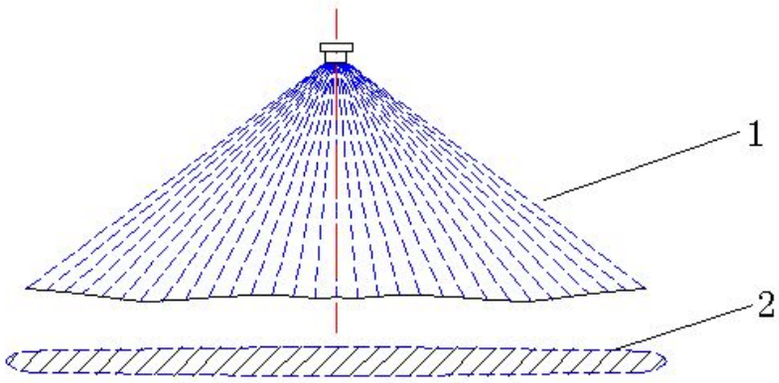

Figure 22. Zonal zones of spray water for flat type nozzle1 is jet stream of flat nozzle, 2 is zonal zones of spray water

As shown in Fig.21, a lot of water droplets will collide crosswise and vertically down between adjacent nozzles. It will lead to water concentration in some area. As shown in Fig.23, The peak phenomenon occurs in water distribution results, and the position of the distance to the edge of slab is 650mm and 1100mm (position of A and B as shown in Fig.21). The experiment proves the validity of the theoretical analysis.

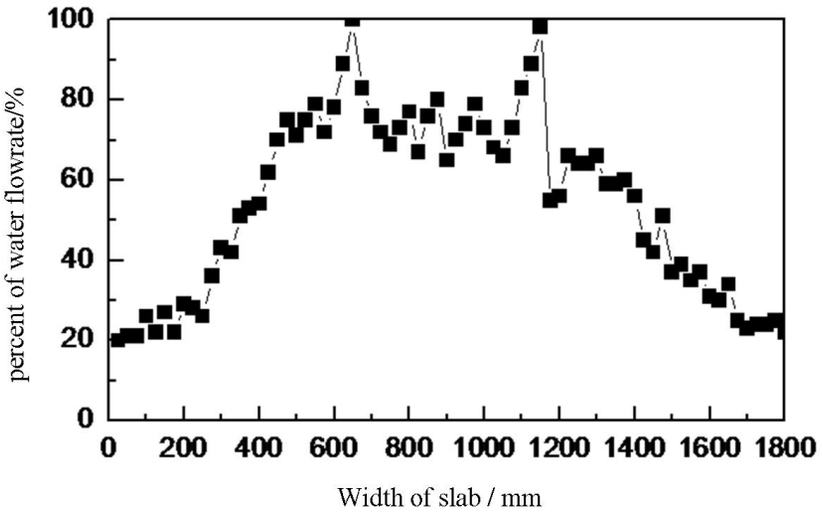

Figure 23. The result of water distributioninjection height: 380mm

In order to avoid water concentration in continuous casting process, it is helpful to prevent water spraying on the same straight line. This will effectively avoid water droplets collide leading to uneven water distribution.

The arrangement of the nozzles is shown in Fig. 24 (a). Considering the restriction of space between rolls, it suggests that the nozzle angle offset is about 5° in this study to make less collide of water spray above the slab if possible. In addition, it can also use the scheme as Fig. 24(b). The length direction of water injection for flat nozzle 1,2,3 are all perpendicular to casting direction. Nozzles of 1, 3 on the edge are located in the same plane. And the nozzle 2 in center is deviated from others a certain distance. This arrangement can also avoid spray water collide between adjacent nozzle.

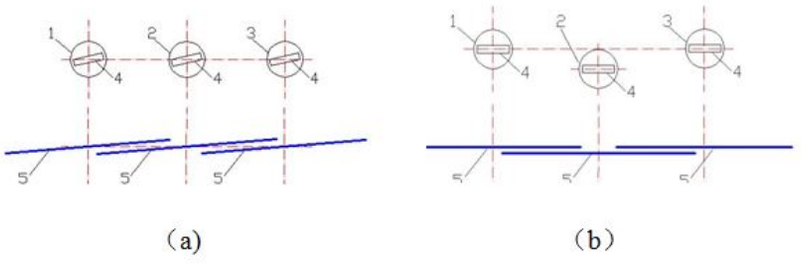

Figure 24. Arrangement of nozzles1,2,3 is the nozzle respectively4 is flat water injection5 is the spray area

After a series of experiments, it shows that the water distribution is more even and will get even cooling in the width direction of slab with above nozzles arrangements.

The control technology of continuous casting of steel not only lies in the fine process model, but also depends on the reasonable production plan. The process of continuous casting should be considered as the linking process between steelmaking process and rolling proc-

http://dx.doi.org/10.5772/51457

ess. The research on casting production plan should be connected with the charge plan and the rolling plan.

5. Planning for the process of steelmaking-rolling

5.1. Models and solutions of planning for the process of steelmaking-rolling

Planning for the process of steelmaking-rolling is programming and decision-making of inventory or contract oriented production by considering the constraints of steel grades, specifics and due dates based on facilities and resources. The production plan could be obtained by integrating optimal charge plan with optimal casting plan and optimal rolling plan. A description of methods and procedures on planning for the process of steelmaking-rolling is described as follows.

5.1.1. The production plan compiling

Generally speaking, the charge (or heat) is the basic unit for the steelmaking process, and a charge represents the whole process. The constraints of steel grades, dimensions and due dates are all considered in the planning process. Therefore, the charge planning problem is a complicated combinatorial optimization problem subjected to several constraints. The optimal charge plan model was developed based on the objective function of the lowest penalties shown as equation (24).

$$\min z = \sum_{j=1}^{n}\left(P_j^1 + P_j^2\right) + \sum_{j=1}^{n}\sum_{p=1}^{0} P_{pj}^3 \cdot X_{pj}$$
$$x_{ik} = \begin{cases} 1 & Contract\ product\ I\ exists\ in\ charge\ k \\ 0 & else \end{cases} \tag{24}$$

In equation (24): n - number of contract products; i,j - serial number of contract products, i, j = 1, 2,…, n; k - serial number of charges, k = 1, 2,…, m;P_k^1 - penalties for contract products unselected into any of the charges,¥; P_k^2- penalties for open order in charge k,; P_{ik}^3- penalties for differences in contract products' due dates in charge k,¥.

Genetic algorithms could be used to solve the model, the basic parameters of the algorithm's evolution algebra, search methods, population size and penalty coefficient should be set firstlythen the iteration calculation should be started with the individual evaluation index of fitness which could be described by penalties, the iteration should be calculated generation by generation until that the smallest value of penalty was obtained, the optimal charge plan could be worked out,then.

The optimal charge plan is obtained by solving the charge plan model with genetic algorithm. The optimal charge plan cannot organize the production independently, the charge

plans must be grouped into multiple casting plans. The casting plan is the rational combination and reasonable sort of the charge plans.

The optimal casting plan model could be established based on two objective functions: minimum total value of penalties for all the casting plans consist of n charge plans shown as equation (25) and maximum average operating rate of continuous casting machines shown as equation (26).

$$\min z_1 = \sum_{i=1}^{m}\sum_{j=1}^{n}\sum_{s=1}^{n}\left(C_{js}^{1} + C_{js}^{2} + C_{js}^{3}\right) \times X_{ij} \times X_{is} \tag{25}$$

$$\max z_2 = \frac{\sum_{i=1}^{m} n_i, t_{i,CCM}}{t^{iE} - t^{iS}} \tag{26}$$

C_{js}^{1}- penalties for production with difference of steel grade between Heat j and Heat s;

C_{js}^{2}- penalties for production with difference of specification between Heat j and Heat s

C_{js}^{3}- penalties for production with difference of due date between Heat j and Heat s

$$X_{i,j} = \begin{cases} 1 & Contract\ product\ I\ exists\ in\ charge\ k \\ 0 & else \end{cases}$$
$$i = 1, 2, ..., n; k = 1, 2, ..., m \tag{27}$$

The optimal casting plan could be obtained by solving this casting plan model with heuristic rules by following steps:

Grouping the charge plans into casts:

The casts could be grouped by steel grade, specification of the items in the charge plans. If the total number of heats in the group exceeds the allowed number of heats of continuous casting machine, the excess heats should be considered as surplus heats.

Sorting the casts by following rules:

Rule 1: the producing steel grade of each cast on the continuous casting machine should be determined by the casts obtained by step (1);

Rule 2: the steel grades and specifications of adjacent casts should be the same as possible;

Rule 3: the casts should be sorted by due date of the order.

Based on the model and calculation above, the optimal grouped casts and optimal casting plan could be obtained.

http://dx.doi.org/10.5772/51457

The optimal rolling plan could be obtained by grouping and sorting the casts in optimal casting plan by the specification ranges and capacity of different mills. The planning process from charge plan to rolling plan is shown in Fig.25.

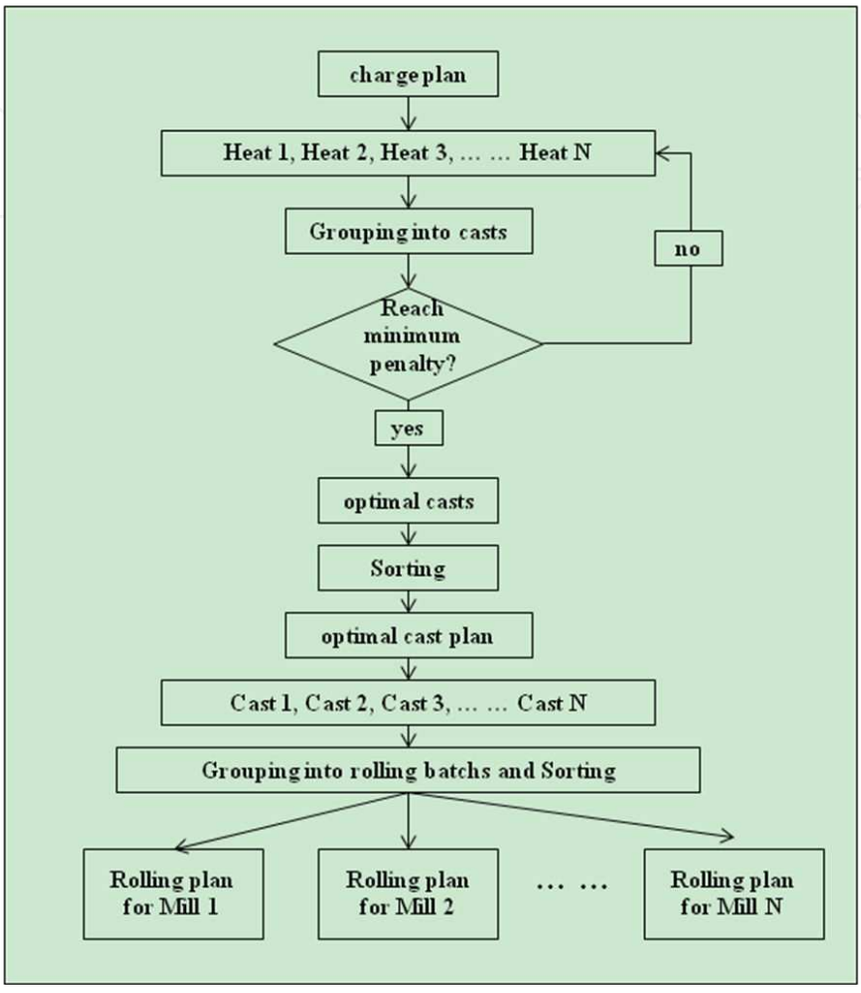

Figure 25. The planning process from charge plan to rolling plan

5.1.2. Buffer and coordination on the plan execution

In order to ensure the stability of the execution of production plan, the rules below should be used when production conflicts and equipment malfunction happened.

1. Rule 1: If the molten steel tapping of some charge delayed, and the delayed time was in the scope of allowed buffer time in refining process, the refining process could take the delayed time as buffer time by prolonging the heating time, and the operating time of continuous casting process and subsequent charges should not be changed;

2. Rule 2: If the molten steel tapping of some charge delayed, and the delayed time was exceed the scope of allowed buffer time in refining process, the refining process could take a part of the delayed time as buffer time by prolonging the heating time, and the

continuous casting process could take the rest of the delayed time as buffer time by lowering the casting speed;

3. Rule 3: If the molten steel tapping of some charge delayed, and the delayed time was exceed the scope of total allowed buffer time in refining process and continuous casting process, the continuous casting machine should stop working;

4. Rule 4: If the continuous casting production of some cast delayed, and the delayed time was in the scope of allowed buffer time in reheating process, the reheating process could take the delayed time as buffer time by changing the heating time and intensity, and the operating time of rolling process should not be changed;

5. Rule 5: If the continuous casting production of some cast delayed, and the delayed time was exceed the scope of allowed buffer time in reheating process, the rolling process should use the intermediate inventory for production.

In the dynamic execution of planning, production conflicts and equipment malfunction could be regulated dynamically by the proposed rules in order to ensure the implementation of the production plan running steadily.

5.2. Examples of planning for the process of steelmaking-rolling

5.2.1. Rule based planning system on the process of steelmaking-rolling in plant A

Based on the analysis of the process of steelmaking-rolling in plant A, a series of rules on planning were proposed, the optimal rule-based plan model was built up. The system was practiced in real productive process. The production mode of plant A is shown as Fig.26, and the window of management of casting plan in the planning system is shown in Fig.27.

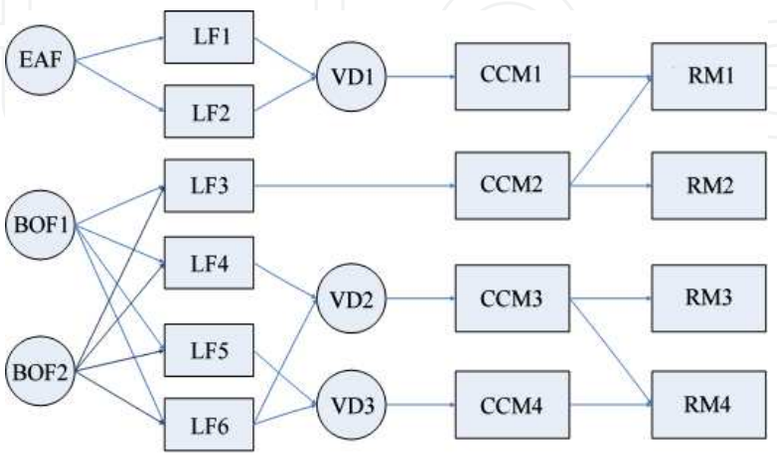

Figure 26. The production mode of plant A

http://dx.doi.org/10.5772/51457

流次	连铸机	钢种	规格	评审号	合同级别	执行标准	定尺	生产数量
1	2#	18CrMnTiH	φ50	0017			6	50
1	2#	20CRMNTIH(TS)	φ50	0141			6	150
2	2#	20CRMNTIH(TS)	φ50	0141			6	100
2	2#	20CRMNTIH(TS)	φ55	0141			6	100
3	2#	20CRMNTIH(TS)	φ55	0141			6	100
3	2#	20CRMNTIH(TS)	φ45	0141			6	100
4	2#	20CRMNTIH(TS)	φ45	0141			6	100
4	2#	20CRMNTIH(TS)	φ40	0141			6	100
5	2#	20CRMNTIH(TS)	φ40	0141			6	100
5	2#	20CrMo	φ25				6	95
5	2#	20CrMo	φ14				6	5
6	2#	20CrMo	φ14				6	85
6	2#	20CrMoA	φ25	0097			8.03	200
7	2#	20CrMoA	φ25	0097			8.03	100
7	2#	20Mn2	φ40				6	20
7	2#	20MnTiB	φ55				6	25
7	2#	20MnTiB	φ25				10.31	175
8	2#	20MnTiB	φ25				10.62	175

Figure 27. The window of management of casting plan in the planning system

This system optimized the planning process combined with SAP management software of plant A, which has the following characteristics:

Firstly, the storage module of planning system closely combined with the third class storage management subsystem of SAP software. The system could eliminate the existed storage production from the requirement list and drop the redundant production to the minimum.

Secondly, the system could analyze the regulation of mass flow of the special steel producing procedure and make arrangements for plan so that the plans would be able to satisfy the mass and energy balance of the productive process.

Thirdly, the system took the productive costs minimum as the goal function, set up the optimized models for each procedure, and so the factory would be able to achieve the goals of reducing costs, improving production quality, shortening producing cycle and delivering goods on time.

5.2.2. Planning and scheduling system on the process of steelmaking-continuous casting in plant B

In this example, planning and scheduling were considered as a whole process to ensure the integrality and systematization of research. The production lines in steelmaking-continuous casting process were optimized on the basis of process analysis, and the optimized production mode was obtained. Planning and scheduling models were established to optimize the total production time, the process waiting time and the operating rate of steelmaking furnaces. Meanwhile, the rule base which was composed of the basic scheduling rules, the equipment selecting rules, the time calculating rules, the manual intervening rules and the real-time adjusting rules, was developed to acquire the scheduling plan shown by Gantt chart (as shown in Fig.28, Gantt chart illustrates the start and finish time of the of each productive mission), and then the dynamic scheduling strategy is explored to cope with the dynamic

events in the production process to ensure the feasibility of the scheduling plan and the stability of the production.

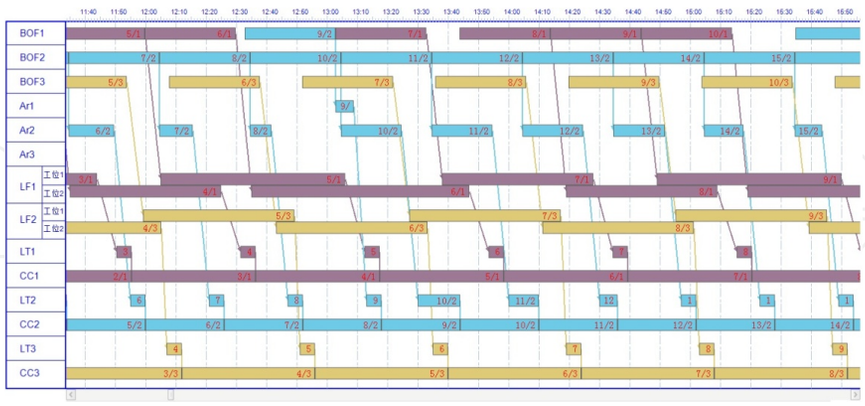

Figure 28. Gantt chart of the process of steelmaking-continuous casting in the system

The planning and scheduling system was established to integrate production planning and scheduling subsystems. The contracts could be converted to the scientific and reasonable scheduling plan by the system, and the conflicts of time or facilities could be eliminated by the dynamic scheduling. The planning and scheduling system showed the efficiency and simplicity of the model and algorithm, the scheduling plan could be obtained within acceptable time, and the proposed solutions could have a great influence on the research of planning and scheduling in steel plants.

Author details

Qing Liu, Xiaofeng Zhang, Bin Wang and Bao Wang

State Key Laboratory of Advanced Metallurgy (University of Science and Technology Beijing; (2)School of Metallurgical and Ecological Engineering, University of Science and Technology Beijing, China

References

[1] Mintz , B. (1999). The influence of composition on the hot ductility of steels and the problem of transverse cracking [J]. *ISIJ International*, 39(9), 833-855.

[2] Yong, Wang, Chunxia, Su, & Yuanpeng, Zhang. (2006). High Temperature Mechanical properties of alloy steel 0.29C-1.20Cr-0.30Ni-0.35Mo [J]. Special Steel (, 27(6), 32-33.

[3] Xiaoqun, He. (2008). Applied Regression Analysis [M]. *Beijing ChinaHigher Education Press*.

[4] Qiaodan, Lu, Zhiyuan, Zhu, Wanjun, Wang, et al. (2002). Influence of calcium treatment on hot ductility of steel for container [J]. *Iron and Steel*, 37(6), 35-38.

[5] Wang, Xin, Wang, Xianyong, Wang, Bao, et al. (2011). Differential Calculation Model for Liquidus Temperature of Steel [J]. *steel research international*, 82(3), 164-168.

[6] Wu, Y. J., Jiang, Z. H., Liang, L. K., et al. (2002). Calculation on Liquidus temperature of Steel [J]. *Journal of Iron and Steel Research*, 14(6), 6-9.

[7] Dong, H. B., & Brooks, R. (2005). Determination of Liquid Journal of Chongqing Univeus temperature in Al-Si and Al-Si-Mg Alloys using a Single-pan Scanning Calorimeter [J]. *Materials Science and Engineering A*, 413, 480-484.

[8] Miettinen, J. (1997). Calculation of solidification-related thermophysical properties for steel [J]. *Metallurgical and Materials Transactions B*, 28B(2), 281-297.

[9] Mills, K. C. (2004). Equations for the Calculation of the Thermophysical Properties of Stainless Steel [J]. *ISIJ International*, 44(10), 1661-1668.

[10] Zhichao, Dou, Liu, Qing, Wang, Bao, et al. (2011). Evolution of Control Models for Secondary Cooling in Continuous Casting Process of Steel [J]. *steel research international*, 82(10), 1220-1227.

[11] Zhao, Jiagui, Qu, Xiuli, Cai, Kaike, et al. (2000). A secondary spray water cooling control model for slab caster and its application [J]. *Metallurgical Industry Automation*, 24(3), 34-36.

[12] Liu, Qing, Wang, Liangzhou, Zhang, Liqiang, et al. (2008). Mathematical model of heat transfer for bloom continuous casting [J]. *Journal of University of Science and Technology Beijing*, 15(1), 17-23.

[13] Chen, Dengfu, Li, Hongliang, Niu, Hongbo, et al. (2007). New Model for Spraying Water of Nozzles in Secondary Cooling of Billet Continuous Casting [J]. *Journal of Chongqing University (Natural Science Edition)*, 30(6), 61-64.

[14] Han, Peng, & Zhang, Xingzhong. (2002). Non-Steady Control of Secondary Cooling Used for Continuous Casting Slab [J]. *Journal of Iron and Steel Research*, 14(4), 73-76.

[15] Gilles, Herbert L. (2003). Primary and Secondary Cooling Control [M] . *The casting volume of the 11th edition of the making, shaping and treating of steel ,AISE*, 33-44.

[16] Kondo, Osamu, Hamada, Katushige, Kuribayashi, Takashi, et al. (1993). New dynamic spray control system for secondary cooling zone of continuous casting machine [M]. *Steelmaking Conference ProceedingsDallas*, 309-314.

[17] Kawasaki, S., Arita, H., Kikunaga, M., Chida, Y., et al. (1984). On the Secondary Cooling Control Technology for the Continuous Casting [J]. *Direct Rolling ProcessNippon Steel Tech-nical Report*, 23, 69-76.

[18] Morita, T., Konishi, M., Kitamura, A., et al. (1986). Control Method of Secondary-Cooling Water for Bloom Continuous Casting. *Kobelco Technical Bulletin*, 1109, 1-5.

[19] Barozzi, P., Fontana, P., & Pragliola, P. (1986). Computer Control and Optimization of Secondary Cooling During Continuous Casting. *Iron and Steel Engineer*, 63(11), 21-26.

[20] Liu, Weitao, Bai, Jubing, Qian, Liang, et al. (2008). Application of Dynamic Secondary Cooling in Continuous Casting of Steel Slab [J]. *Foundry Technology* [12], 1651-1654.

[21] Guo, Liangliang, Tian, Yong, yao, Man, et al. (2009). Temperature distribution and dynamic control of secondary cooling in slab continuous casting [J]. *International Journal of Minerals, Metallurgy and Materials*, 16(6), 626-631.

[22] Zhang, Zheng Shan, Chai, Tianyou, Wang, Wei, et al. (1999). Secondary cooling control for alloy steel billet continuous caster in Fushun Special Steel Co Ltd [J]. Metallurgical Industry Automation, , , 23(5), 32-35.

[23] Takawa, T., Takahashi, R., & Tatsuwaki, M. (1987). Mathematical Model and Control System of Cooling Process. *The Sumitomo Search*, 34, 79-87.

[24] Morwald, K., Dittenberger, K., & Ives, K. D. (1998). Dynacs cooling system-features and operational results [J] . *Ironmaking & Steelmaking*, 25(4), 323-327.

[25] Hardin, Richarda, Liu, Kai, Kapoor, Atul, et al. (2003). A transient simulation and dynamic spray cooling control model for continuous steel casting. *Metallurgical and Materials Transactions B*, 34B(3), 297-306.

[26] Okuno, K., Naruwa, H., & Kuribayashi, T. (1987). Dynacs spray cooling control system for continuous casting [J]. *Iron and Steel Engineer*, 64(4), 34-38.

[27] Spitzer, K.H., Harste, K., Weber, B., et al. (1992). Mathematical model for thermal tracking and on-line control in continuous casting [J]. *ISIJ International*, 32(7), 848-856.

[28] Camisani-Calzolari, F.R., Craig, I.K., & Pistorius, P.C. (2000). Speed disturbance compensation in the secondary cooling zone in continuous casting [J]. *ISIJ International*, 40(5), 469-477.

[29] Liu, Wen-kai, Xie, Zhi, Ji, Zhen-ping, et al. (2008). Dynamic water modeling and application of billet continuous casting [J]. *Journal of Iron and Steel Research International*, 15(2), 14-17.

[30] Cai, Ji, Zhang, Shuyan, zhao, Qi, et al. (2005). Study and implement of real-timperature field calculation and secondary cooling control model for slab caster with dynamic soft reduction [M]. *CSM 2005 Annual Meeting Proceedings, Beijing*, 3, 340-345.

[31] Xianyong, Wang, Qing, Liu, & Zhigang, Hu. (2010). Influence of nozzle layouts on the secondary cooling effect ofmedium thickness slabs i n continuous casting [J]. *Journal of University of Science and Technology Beijing*, 32(8).

[32] Wang, Xianyong, Liu, Qing, Wang, Xin, et al. (2011). Optimal control of secondary cooling for medium-thickness slab continuous casting. *Ironmaking & Steelmaking [J]*, 38(7), 552-560.

[33] Qing, Liu. (2002). Research on mode optimization of modern BOF steelmaking workshop for long products-the effect of high efficiency continuous casting technology on running control for modern BOF steelmaking workshop. *Beijing: University of Science and Technology Beijing*.

[34] Qing, Liu, Bai, Suhong, Lu, Junhui, et al. (2008). Production plan schedule for the casting-rolling process in BOF special steel plants [J]. *Journal of University of Science and Technology Beijing*, 30(5), 566-570.

[35] Bin, Wang. (2009). Research on planning and dispatching of steelmaking-rolling process at Shijiazhuang iron and sSteel corporation [D]. *Beijing: University of Science and Technology Beijing*.

[36] Chuang, Wang. (2012). Research on production planning and scheduling system for steelmaking-continuous casting process in the special steel workshop [D]. *Beijing: University of Science and Technology Beijing.*

[37] Gantt, H. L. (1910). Work, Wages, Profit. The management of projects [M]. *The Engineering Magazine, New York.*

IntechOpen